



Numerical investigations on magnetic field modeling for Carreau non-Newtonian fluid flow past an isothermal sphere

CH. Amanulla¹ · Abderrahim Wakif² · Zoubair Boulahia² · M. Suryanarayana Reddy³ · N. Nagendra⁴

Received: 16 November 2017 / Accepted: 22 August 2018 / Published online: 31 August 2018
© The Brazilian Society of Mechanical Sciences and Engineering 2018

Abstract

In the current study, the effects of radial magnetic field, slip and jump conditions on the steady two-dimensional free convective boundary layer flow over an external surface of an isothermal sphere for an electro-conductive polymer are numerically studied. It is assumed that the studied fluid has a non-Newtonian rheological behavior and follows the Carreau fluid model. In this investigation, the formulation of the Carreau fluid model has been used first time for describing the present boundary layer problem, and then the resulting partial differential equations are transformed to ordinary differential equations by using non-similarity transformations. The obtained ordinary differential equations are solved numerically by a well-known method named as Keller-Box method. The finding results show that a weak elevation in temperature is accompanied with the increase in the Carreau fluid parameter, whereas a significant acceleration in the flow is computed near the sphere surface. It is shown also that an increase in the thermal slip parameter allows to strongly decrease both the skin friction coefficient and the local Nusselt number. The skin friction coefficient is also depressed with increasing magnetic body force parameter. Moreover, it is observed that an increase in the momentum slip parameter allows to decrease the skin friction coefficient, whereas the local Nusselt number is reduced with the increase in the Carreau fluid parameter. It is found also that the skin friction coefficient is increased with greater stream-wise coordinate, whereas the local Nusselt number is reduced with the increase in this parameter.

Keywords Magnetohydrodynamics · Carreau fluid · Keller-Box method · Velocity slip · Temperature jump

List of symbols

a Radius of the sphere, m
 B_0 Externally imposed radial magnetic field
 c Specific heat, $\text{J kg}^{-1} \text{K}^{-1}$
 C_f Skin friction coefficient ($C_f = a^2 \tau_w / (\rho v^2)$)
 f Dimensionless stream function
($f = \psi / (v \xi Gr^{1/4})$)

Gr Grashof number ($Gr = g \beta (T_w - T_\infty) a^3 / \nu^2$)
 \mathbf{g} Gravity field
 k Thermal conductivity of fluid, $\text{W m}^{-1} \text{K}^{-1}$
 n Power law index parameter
 K_0 Thermal jump factor, m^{-1}
 N_0 Momentum slip factor, m^{-1}
 Nu Local Nusselt number
($Nu_x = -a (\partial T / \partial y)_{y=0} / (T_w - T_\infty)$)
 M Magnetic parameter ($M = \sigma a^2 B_0^2 / (\rho \nu Gr^{1/2})$)
 P Pressure, Pa
 Pr Prandtl number ($Pr = \nu / \alpha$)
 S_f Velocity slip parameter ($S_f = N_0 Gr^{1/4} / a$)
 S_T Thermal jump parameter ($S_T = K_0 Gr^{1/4} / a$)
 T Temperature, K
 U, V Dimensionless velocity components, m s^{-1}
 We Weissenberg number ($We = (\Gamma \nu x Gr^{3/4} / a^3)^2$)
 x Stream-wise coordinate, m
 y Transverse coordinate, m

Technical Editor: Cezar Negrao.

✉ CH. Amanulla
amanullams@gmail.com

¹ Department of Mathematics, Jawaharlal Nehru Technological University, Anantapur, Anantapuramu 515002, India

² Faculty of Sciences Ain Chock, Laboratory of Mechanics, Hassan II University, B.P.5366, Mâarif, Casablanca, Morocco

³ Department of Mathematics, JNTUA College of Engineering, Pulivendula, Andhra Pradesh, India

⁴ Department of Mathematics, Madanapalle Institute of Technology and Science, Madanapalle, India

Greek symbols

α	Thermal diffusivity, $\text{m}^2 \text{s}^{-1}$
β	Thermal expansion coefficient, K^{-1}
η	Dimensionless transverse coordinate ($\eta = yGr^{1/4}/a$)
θ	Dimensionless temperature ($\theta = (T - T_\infty) / (T_w - T_\infty)$)
μ_0	Zero shear rate viscosity, Pa s
ν	Kinematic viscosity ($\nu = \mu_0 / \rho$), $\text{m}^2 \text{s}^{-1}$
ξ	Dimensionless stream-wise coordinate ($\xi = x/a$)
ρ	Fluid density, Kg m^{-3}
σ	Electrical conductivity, $\Omega^{-1} \text{m}^{-1}$
τ_w	Wall shear stress ($\tau_w = \mu_0(\partial U/\partial y) _{y=0} + \mu_0(n-1)(\Gamma^2/2)(\partial U/\partial y)^3 _{y=0}$)
ψ	Stream function, $\text{m}^2 \text{s}^{-1}$
Γ	Time-dependent material constant, s
Δ	Nabla operator

Subscripts

w	Wall condition
∞	Free stream condition

1 Introduction

A good recognition gained by the non-Newtonian fluid in the hydraulic machinery helps researchers and engineers to improve the work productivity in various fields such as drive engineering, automotive, construction, agricultural, mining, petrochemical industries, and power plant construction. For instance, the usage of the non-Newtonian lubricant in the bearings maximizes its effectiveness in the process pumps. A few salt arrangements and liquid polymers are non-Newtonian liquids, as are numerous different fluids experienced in science and innovation, for example, dental creams, physiological liquids, cleansers and paints. In a non-Newtonian liquid, the connection between the shear stretch and the shear rate is by and large non-direct and can even be time subordinate. The Carreau model although simple is useful in simulating a number of polymers. Coating hydrodynamics has been an area of considerable interest, since Landau and Levich [1] have published in their pioneering work in 1942, in which an elegant formulation was developed for the thickness of the Newtonian viscous fluid films, which is deposited on a plate withdrawn vertically from a bath at a constant velocity. Lawrence and Zhou [2] have reported in their interesting investigation that the non-Newtonian polymer fluids are encountered in many modern industries, especially in the polymer coating processes. Numerous researchers have investigated the coating dynamics of different geometrical bodies (plates, cones, spheres, cylinders) with non-

Newtonian liquids and have employed a range of mathematical constitutive equations. Jenekhe and Schuldt [3] have studied the coating flows of power law and Carreau fluids on spinning disks. Campanella et al. [4] have treated the dip coating of a circular cylinder in non-Newtonian power law fluids. Zevallos et al. [5] have used the finite element for simulating the forward roll coating flows for viscoelastic liquids using both Oldroyd-B and FENE-P models. However, these studies ignored the heat transfer which may be critical in certain coating systems. This remark has been confirmed by Mitsoulis [6] and Mark [7]; they have shown in their research papers that the diffusion of heat can modify the polymer properties significantly.

For portraying the non-Newtonian stream conduct, Navier–Stokes conditions are insufficient. We require some physical models to fill this hole, for example, the Cross and Ellis display, the Carreau show, the Casson demonstrate, and so on. Non-Newtonian liquids are extremely useful in glass blowing, optimal design, paper creation, consistent throwing, and so on. The use of physical states of non-Newtonian liquid streams is directly trying for researchers, mathematicians and physicists, in viable and in addition hypothetical examinations. The explanation for this is these liquids are exceptionally perplexing in nature and there is no specific constitutive condition for speaking to all stream properties of non-Newtonian liquids. In Carreau liquids, the thickness is lessened with rising shear stretch rates. This model has discovered some fame in building reenactments. Hashim and Masood [8] scrutinized the multiple solutions for the Carreau fluid flow over a shrinking cylinder. The influence of the magnetic field on the stagnation-point flow and heat transfer of Carreau fluid over a convectively heated surface has been theoretically reviewed by Khan et al. [9]. By keeping this into view, the researchers of [10–14] analyzed the non-Newtonian fluid flow properties by considering the various flow geometries and different physical effects. Wall slip in thermal polymer processing was considered by Liu and Gehde [15] in which slip was shown to significantly modify temperature distribution in polymers. Hatzikiriakos and Mitsoulis [16] presented closed form solutions and finite element computations for wall slip effects on pressure drop of power law fluids in tapered dies. Many studies of both momentum (hydrodynamic or velocity) slip and thermal slip on transport phenomena have also been reported. Amanulla et al. [17, 18] have used the MATLAB software to compute the influence of momentum and thermal jump convective conditions on two-dimensional viscoelastic boundary layers in nanofluid flows over a sphere. Sparrow et al. [19] presented the first significant analysis of laminar slip-flow heat transfer for tubes with uniform heat flux, observing that momentum slip acts to improve heat transfer

whereas thermal slip (or temperature jump) reduces heat transfer.

Among the interesting viscoelastic model in non-Newtonian fluid mechanics we find the Carreau fluid model, which is degenerated to a Newtonian fluid at a very high wall shear stress. This model approximates reasonably well the rheological behavior of a wide range of industrial liquids including biotechnological detergents, physiological suspensions, foams, geological material, cosmetics and syrups. Many researchers have explored a range of industrial and biological flow problems using the Carreau model. Khellaf and Lauriat [20] investigated the Carreau fluid flow and heat transfer between two concentric cylinders. Khan et al. [21] analyzed the MHD non-Newtonian Carreau fluid flow over a convective surface with non-linear radiative heat transfer effects. Raju and Sandeep [22] examined the heat and mass transfer in Falkner–Skan Carreau fluid flow past an isothermal wedge. MHD stagnation-point flow of Carreau fluid over a shrinking sheet is studied theoretically by Akbar et al. [23]. The steady radiative MHD free convection flow of a Carreau fluid from a shrinking sheet with magnetic field, thermal and concentration slip has been investigated by Reddy and Sandeep [24]. Furthermore, this model utilizes time derivatives rather than converted derivatives, which facilitates numerical solutions in boundary value problems.

The previous studies invariably assumed the classical boundary conditions. However, the slip effects have shown to be important in numerous polymeric transport processes including the production stage of polymers from the raw materials. Black [25] has reported that the slip effect on the wall must be taken into account during converting high molecular weight products into specific products. Consequently, many researchers, primarily in chemical engineering, have studied experimentally and numerically the influence of wall slip on polymer dynamics. The important works in this regard include Wang et al. [26] who considered low density polyethylene liquids, Piau et al. [27] who addressed polymer extrudates, Piau and Kissi [28] who quantified macroscopic wall slip in polymer melts, Lim and Schowalter [29] who studied boundary slip in polybutadiene flows and Hatzikiriakos and Kalogerakis [30] who studied molten polymer wall slip. The wall slip in thermal polymer processing was considered by Liu and Gehde [15], in which the slip was shown to significantly modify temperature distribution in polymers. Hatzikiriakos and Mitsoulis [16] have presented closed form solutions and finite element computations for wall slip effects on pressure drop of power law fluids in tapered dies. Many studies of the effects of both the momentum slip (i.e., velocity slip) and the thermal slip on transport phenomena have also been reported. Sparrow et al. [31] have presented the first significant analysis of laminar slip-flow heat transfer for tubes with uniform heat

flux. They have observed that the momentum slip acts to improve the heat transfer, whereas the thermal slip (i.e., temperature jump) reduces the heat transfer. Ali and Khan [32] studied exact solution of MHD free convection slip flow and heat transfer over a porous plate in the presence of heat flux. Aziz et al. [33] examined the slip effect on boundary layer flow of power law fluid including heat transfer over a porous flat sheet embedded in a porous medium. Ellahi et al. [34] work on hall and ion slip on MHD peristaltic flow of an elastic viscous fluid from a rectangular duct. Recently, the researchers [35–40] discussed the non-Newtonian fluid flow of vertical surfaces with velocity and temperature jump boundary conditions. In these studies, they found very interesting solutions as the momentum slip and thermal slip parameter has tendency to control the skin friction and local Nusselt number profiles and also the non-Newtonian fluids are regulating the temperature profiles of the flow.

All the above studies have focused on the flow over a plane, over a parabolic leading edge parabolic or in many other regions. In this work, we investigate numerically the two-dimensional MHD Carreau fluid flow over a sphere in the presence of velocity and thermal slip effects, using the Keller-Box numerical method. The impact of different parameters on the fluid flow, thermal fields, skin friction and rate of heat transfer is shown graphically. The results are presented in tabular form to discuss the wall friction and the reduced local Nusselt number.

2 Formulation of the problem

Consider the steady laminar boundary layer flow of two-dimensional incompressible Carreau fluid over an isothermal spherical body of fixed radius a , in the presence of a uniform radial magnetic field \mathbf{B}_0 . In this investigation, the induced magnetic field, the Hall effect and the viscous and Joule dissipation terms are assumed to be negligible, so that the surface temperature of the sphere T_w is taken greater than the ambient temperature of the fluid T_∞ . (e.g., heated sphere). The physical model considered is illustrated in Fig. 1.

Following Akbar et al. [10, 23], Molla et al. [41] and Haque et al. [42], the differential equations governing the present problem are given as follows:

$$\nabla \cdot \mathbf{V} = 0 \quad (1)$$

$$\rho \left[\frac{\partial \mathbf{V}}{\partial t} + (\mathbf{V} \cdot \nabla) \mathbf{V} \right] = -\nabla P + \nabla \cdot \bar{\tau} + \rho \mathbf{g} + \sigma (\mathbf{V} \times \mathbf{B}_0) \times \mathbf{B}_0 \quad (2)$$

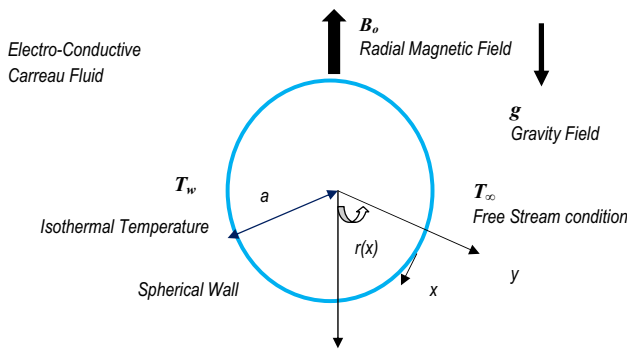


Fig. 1 Magnetohydrodynamic non-Newtonian heat transfer from a sphere

$$\rho c \left[\frac{\partial T}{\partial t} + (\mathbf{V} \cdot \nabla) T \right] = -\nabla \cdot \mathbf{q} \tag{3}$$

Here, \mathbf{V} is the velocity vector, $\bar{\tau}$ is the extra stress tensor, \mathbf{q} is the heat flux vector, where $\mathbf{V} = (U, V)$ and $\mathbf{q} = -k\nabla T$.

In the case where the infinite shear rate viscosity μ_∞ of this kind of non-Newtonian fluids is neglected (i.e., $\mu_\infty \approx 0$), the extra stress tensor $\bar{\tau}$ is defined as:

$$\bar{\tau} = \mu_0 \left(1 + (\Gamma \dot{\gamma})^2 \right)^{\frac{(n-1)}{2}} \left(\bar{\mathbf{L}} + \bar{\mathbf{L}}^T \right) \tag{4}$$

Here μ_0 is the zero shear rate viscosity, Γ is the time constant, n is the power law index, $\dot{\gamma}$ is the shear rate and $\bar{\Pi}$ is the second invariant strain rate tensor (i.e., $\bar{\Pi} = \text{trace} \left[\left(\bar{\mathbf{L}} + \bar{\mathbf{L}}^T \right)^2 \right]$), where $\bar{\mathbf{L}} = \nabla \mathbf{V}$ and $\dot{\gamma} = \sqrt{\frac{1}{2} \bar{\Pi}}$.

We consider in the constitutive Eq. (4) the case for which $\Gamma \dot{\gamma} \ll 1$, so we can write:

$$\bar{\tau} = \mu_0 \left(1 + \frac{(n-1)}{2} (\Gamma \dot{\gamma})^2 \right) \left(\bar{\mathbf{L}} + \bar{\mathbf{L}}^T \right) \tag{5}$$

Under the Boussinesq and boundary layer approximations, the simplified steady governing equations are expressed as follows:

$$\frac{\partial(Ur)}{\partial x} + \frac{\partial(Vr)}{\partial y} = 0 \tag{6}$$

$$U \frac{\partial U}{\partial x} + V \frac{\partial U}{\partial y} = g\beta(T - T_\infty) \sin\left(\frac{x}{a}\right) - \frac{\sigma B_0^2}{2} U + \nu \frac{\partial^2 U}{\partial y^2} + \nu \frac{3(n-1)\Gamma^2}{2} \left(\frac{\partial U}{\partial y} \right)^2 \frac{\partial^2 U}{\partial y^2} \tag{7}$$

$$U \frac{\partial T}{\partial x} + V \frac{\partial T}{\partial y} = \alpha \frac{\partial^2 T}{\partial y^2} \tag{8}$$

Rewriting Eqs. (6)–(8) in terms of the stream function ψ (i.e., $Ur = \partial(r\psi)/\partial y$ and $Vr = -\partial(r\psi)/\partial x$), $r = a \sin(x/a)$ is the radial distance from the symmetrical axis to the surface of the sphere and the temperature T .

Considering the case of presence of velocity slip and temperature jump conditions at the cylindrical exterior wall, we can write the boundary conditions imposed to the system of Eqs. (8) and (9) as follows:

$$u = N_0 \frac{\partial u}{\partial y}, \quad v = 0, \quad T = T_w + K_0 \frac{\partial T}{\partial y} \quad \text{at } y = 0 \tag{9}$$

The parameters N_0 and K_0 used in the boundary conditions (6) represent the thermal jump and momentum slip factors, respectively. For recovering the no-slip case, one can take $N_0 = K_0 = 0$.

In order to write the governing equations and the boundary conditions in dimensionless form, the following non-dimensional quantities are introduced:

$$\xi = \frac{x}{a}, \quad \eta = \frac{y}{a} Gr^{1/4}, \quad f(\xi, \eta) = \frac{\psi}{\nu \xi Gr^{1/4}}, \quad \theta(\xi, \eta) = \frac{T - T_\infty}{T_w - T_\infty} \tag{10}$$

By applying the non-similar transformations of Eq. (12) on the system of Eqs. (9)–(11), we obtain:

$$f'''(\eta) + (1 + \xi \cot \xi) f f''(\eta) + \frac{3(n-1) We}{2} (f''(\eta))^2 f'''(\eta) - (f(\eta))^2 + \frac{\sin(\xi)}{\xi} \theta - M f(\eta) = \xi \left(f'(\eta) \frac{\partial f''(\eta)}{\partial \xi} - f''(\eta) \frac{\partial f}{\partial \xi} \right) \tag{11}$$

$$Pr^{-1} \theta''(\eta) + (1 + \xi \cot \xi) f \theta'(\eta) = \xi \left(f'(\eta) \frac{\partial \theta}{\partial \xi} - \theta'(\eta) \frac{\partial f}{\partial \xi} \right) \tag{12}$$

$$f = 0, \quad f'(\eta) = S_f f''(\eta), \quad \theta = 1 + S_T \theta'(\eta) \quad \text{at } \eta = 0$$

$$f' \rightarrow 0, \quad \theta \rightarrow 0 \quad \text{as } \eta \rightarrow \infty \tag{13}$$

The skin friction coefficient C_f and the local Nusselt number Nu_x can be found using the following expressions:

$$Gr^{-3/4} C_f = \xi f''(\xi, 0) \left(1 + \frac{(n-1) We}{2} f''^2(\xi, 0) \right) \tag{14}$$

$$Gr^{-1/4} Nu_x = -\theta'(\xi, 0) \tag{15}$$

3 Computational solution with Keller-Box implicit method

The coupled boundary layer equations in a (ξ, η) coordinate system remain strongly nonlinear. An efficient implicit finite difference method, called the Keller-Box scheme, is therefore used as numerical technic to solve the boundary value problem defined by Eqs. (11) and (12) with the boundary conditions (13). This technique has been described succinctly in Cebeci and Bradshaw [43] and Keller [44]. It has been used recently in polymeric flow dynamics by Amanulla et al. [35–38, 48] for viscoelastic models and Rao et al. [45–47] for non-Newtonian fluids. Very few of these papers, however, have provided guidance for researchers as to customization of the Keller-Box scheme to heat transfer problems. We have included the full details for discretizing the present problem with this procedure, so that the implementation of Keller’s scheme involves the following steps:

- (a) Reduction of the N th order corresponding to the system of partial differential equations to a set of N first order equations.
- (b) Discretization of the obtained first-order equations with finite difference schemes.
- (c) Quasilinearization of the nonlinear Keller algebraic equations.
- (d) Solve the system of linear Keller algebraic equations using an efficient block tridiagonal elimination procedure.

Considering the following change of variables:

$$f' = u \tag{16}$$

$$u' = v \tag{17}$$

$$\theta' = t \tag{18}$$

Equations (11) and (12) can be reduced to the following form:

$$v' + (1 + \xi \cot \xi)fv + \frac{3(n-1)We}{2}vv' - u^2 + \frac{\sin(\xi)}{\xi}s - Mu = \xi \left(u \frac{\partial u}{\partial \xi} - v \frac{\partial f}{\partial \xi} \right) \tag{19}$$

$$Pr^{-1}t' + (1 + \xi \cot \xi)ft = \xi \left(u \frac{\partial s}{\partial \xi} - t \frac{\partial f}{\partial \xi} \right) \tag{20}$$

Here, the primes denote differentiation with respect to η and $\theta = s$.

In terms of the dependent variables, the boundary conditions (13) become:

$$f = 0, f' = S_f f''(0), \theta = 1 + S_T \theta'(0) \text{ at } \eta = 0$$

$$f' \rightarrow 0, \theta \rightarrow 0 \text{ as } \eta \rightarrow \infty \tag{21}$$

A two-dimensional computational mesh is imposed on the $\xi-\eta$ plane as shown in Fig. 2. The stepping process is defined by:

$$\eta_0 = 0, \eta_j = \eta_{j-1} + h_j, 1 \leq j \leq J, \eta_J \equiv \eta_\infty \tag{22}$$

$$\zeta^0 = 0, \zeta^n = \zeta^{n-1} + k_n, 1 \leq n \leq N \tag{23}$$

Here, k_n and h_j denote the step distances in the ξ and η directions, respectively.

If g_j^n denotes the value of any variable at (η_j, ζ^n) , then the variable and derivative terms appeared in Eqs. (19) and (20) at $(\eta_{j-1/2}, \zeta^{n-1/2})$ are replaced by:

$$g_{j-1/2}^{n-1/2} = \frac{1}{4} (g_j^n + g_{j-1}^n + g_j^{n-1} + g_{j-1}^{n-1}) \tag{24}$$

$$\left(\frac{\partial g}{\partial \eta} \right)_{j-1/2}^{n-1/2} = \frac{1}{2h_j} (g_j^n - g_{j-1}^n + g_j^{n-1} - g_{j-1}^{n-1}) \tag{25}$$

$$\left(\frac{\partial g}{\partial \xi} \right)_{j-1/2}^{n-1/2} = \frac{1}{2k^n} (g_j^n - g_{j-1}^n + g_j^{n-1} - g_{j-1}^{n-1}) \tag{26}$$

The finite difference approximations at the mid-point $(\eta_{j-1/2}, \zeta^n)$ for the variables u, v and t are given as:

$$h_j^{-1} (f_j^n - f_{j-1}^n) = u_{j-1/2}^n \tag{27}$$

$$h_j^{-1} (u_j^n - u_{j-1}^n) = v_{j-1/2}^n \tag{28}$$

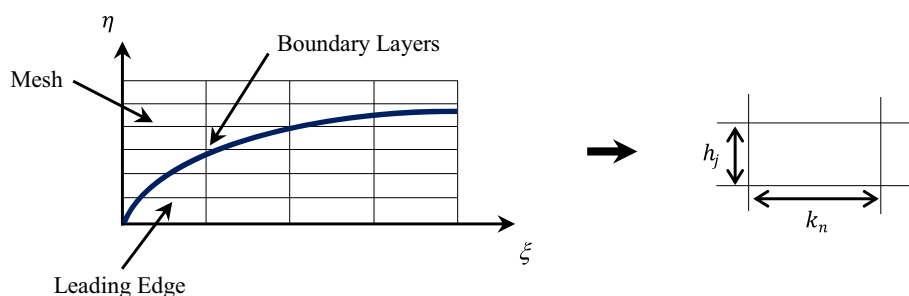
$$h_j^{-1} (s_j^n - s_{j-1}^n) = t_{j-1/2}^n \tag{29}$$

Hence, the appropriate discretized form of Eqs. (19) and (20) are written as follows:

$$(v_j - v_{j-1}) + (1 + \alpha + \xi \cot \xi) \frac{h_j}{4} (f_j + f_{j-1})(v_j + v_{j-1}) - \frac{(1 + \alpha)h_j}{4} (u_j + u_{j-1})^2 + \frac{3(n-1)We}{4} [(v_j)^2 - (v_{j-1})^2] + \frac{Ah_j}{2} (s_j + s_{j-1}) - \frac{Mh_j}{2} (u_j + u_{j-1}) - \frac{\alpha h_j}{2} f_{j-1/2}^{n-1} (v_j + v_{j-1}) + \frac{\alpha h_j}{2} v_{j-1/2}^{n-1} (f_j + f_{j-1}) = [R_1]_{j-1/2}^{n-1} \tag{30}$$

$$Pr^{-1} (t_j - t_{j-1}) + (1 + \alpha + \xi \cot \xi) \frac{h_j}{4} [(f_j + f_{j-1})(t_j + t_{j-1})] - \frac{\alpha h_j}{4} [(u_j + u_{j-1})(s_j + s_{j-1})] + \frac{\alpha h_j}{2} s_{j-1/2}^{n-1} (u_j + u_{j-1}) - \frac{\alpha h_j}{2} u_{j-1/2}^{n-1} (s_j + s_{j-1}) - \frac{\alpha h_j}{2} f_{j-1/2}^{n-1} (t_j + t_{j-1}) + \frac{\alpha h_j}{2} t_{j-1/2}^{n-1} (f_j + f_{j-1}) = [R_2]_{j-1/2}^{n-1} \tag{31}$$

Fig. 2 Keller-Box element and boundary layer mesh



Here, the following abbreviations are used:

$$\alpha = \frac{\zeta^{n-1/2}}{k_n}, A = \frac{\sin\left(\frac{\zeta^{n-1/2}}{k_n}\right)}{\zeta^{n-1/2}} \quad (32)$$

$$\begin{aligned} \frac{-[R_1]_{j-1/2}^{n-1}}{h_j} &= \left(\frac{v_j - v_{j-1}}{h_j}\right) + (1 - \alpha + \zeta \cot \xi) (f_{j-1/2} v_{j-1/2}) \\ &+ \frac{3(n-1) We}{2} (v_{j-1} v'_{j-1/2}) + (1 - \alpha) (u_{j-1/2})^2 \\ &+ A s_{j-1/2} - M u_{j-1/2} \end{aligned} \quad (33)$$

$$\begin{aligned} \frac{-[R_2]_{j-1/2}^{n-1}}{h_j} &= Pr^{-1} \left(\frac{t_j - t_{j-1}}{h_j}\right) \\ &+ (1 - \alpha + \zeta \cot \xi) (f_{j-1/2} t_{j-1/2}) \\ &+ \alpha (u_{j-1/2} s_{j-1/2}) \end{aligned} \quad (34)$$

The system of Eqs. (30) and (31) is solved subject to the following boundary conditions:

$$f_0^n = u_0^n = 0, \theta_0^n = 1, u_J^n = 0, v_J^n = 0, \theta_J^n = 0 \quad (35)$$

The emerging nonlinear system of algebraic equations is linearized by means of Newton’s method and then solved by the block elimination procedure. The accuracy of computations is influenced by the number of mesh points in both directions. After experimenting with various grid sizes in the η direction a larger number of mesh points are selected whereas in the ζ direction significantly less mesh points are utilized. The numerical value of η_{max} has been set at 10, and this defines a sufficiently large value at which the prescribed boundary conditions are satisfied, whereas the limited value ζ_{max} is set at 3 for this flow domain. Mesh independence is therefore achieved in the present computations. The present problem is solved using the Keller-Box finite difference scheme with the help of software MATLAB.

Assuming that $f_{j-1}^{n-1}, u_{j-1}^{n-1}, v_{j-1}^{n-1}, s_{j-1}^{n-1}$ and t_{j-1}^{n-1} are known for $1 \leq j \leq J$, the discretized Eqs. (29)–(33) constitute a system of $5J + 5$ equations, which is composed by the $5J + 5$ unknowns $f_j^n, u_j^n, v_j^n, s_j^n$ and t_j^n , where $0 \leq j \leq J$. The resulting nonlinear system of algebraic equations is

linearized by means of Newton’s method, and then solved in a very efficient manner by using the Keller-Box method, which has been explained more clearly by Cebeci and Bradshaw [43], taking the initial interaction with a given set of converged solutions at $\zeta = \zeta^n$. To initiate the process with $\zeta = 0$, we first prescribe a set of guess profiles for the functions f, u, v, s and t which are unconditionally convergent. These profiles are then employed in the Keller-Box scheme with second-order accuracy to compute the correct solution step by step along the boundary layer. For a given ζ the iterative procedure is stopped to give the final velocity and temperature distributions when the difference in computing of these functions in the next procedure become less than 10^{-5} , i.e., $|\delta f^i| \leq 10^{-5}$, where the superscript i denotes the number of iterations. For laminar flows, the rate of convergence of the solutions for Eqs. (29)–(33) is quadratic provided the initial estimate to the desired solution is reasonably close to the final solution. Calculations are performed with four different $\Delta\eta$ spacing showing that the rate of convergence of the solutions is quadratic in all cases for these initial profiles with typical iterations. The fact that Newton’s method is used to linearize the nonlinear algebraic equations and that with proper initial guess ζ^n usually obtained from a solution at ζ^{n-1} , the rate of convergence of the solutions should be quadratic, it can be used to test the code for possible programming errors and to aid in the choice of the spacing $\Delta\zeta$ in the downstream direction. To study the effect of the spacing $\Delta\zeta$ on the rate of convergence of solutions, calculations were performed in the range $0 \leq \zeta \leq 0.4$ with uniform spacing $\Delta\zeta$ corresponding to 0.08, 0.04, 0.02 and 0.01. Except for the results obtained with $\Delta\zeta = 0.08$, the rate of convergence of the solutions was essentially quadratic at each ζ station. In most laminar boundary layer flows, a step size from 0.02 to 0.04 is sufficient to provide accurate and comparable results. In fact in the present problem, we can even go up to $\Delta\zeta = 0.1$ and still get accurate and comparable results. This particular value of $\Delta\zeta = 0.1$ has also been used successfully by Molla et al. [41]. A uniform grid across the boundary is quite satisfactory for most laminar flow calculations, especially in laminar boundary layer. However, the Keller-Box method

is unique in which various spacing in both η and ξ directions can be used.

4 Numerical results and interpretation

In order to verify the accuracy of the Keller-box method solutions, computations are benchmarked with earlier results reported by Molla et al. [41] and Haque et al. [42], via the values of the skin friction and heat transfer coefficients C_f and Nu_x of a Newtonian fluid (i.e., $We = 0$), respectively, for various values of the parameter ξ , in the case where $Pr = 1, S_f = 0, S_T = 0$ and $M = 0$.

The results of this comparison are summarized in Table 1. Very close correlation is achieved between the Keller-Box computational results and the solutions of Molla et al. [41] and Haque et al. [42]. Hence, the Keller-Box numerical code used in this investigation leads to quite accurate numerical results. In order to give the truthfulness and reliability to the numerical method used in this investigation, we present in Tables 2, 3, 4 and 5 the numerical values of the quantities $f''(\xi, 0)$ and $-\theta'(\xi, 0)$, which are obtained after many computational tests, for various values of the parameters S_f, S_T, ξ, We, M and Pr .

The effects of major controlling parameters on the profiles of the functions $f'(\xi, \eta), \theta(\xi, \eta), Gr^{-3/4} C_f$ and $Gr^{-1/4} Nu$ are analyzed graphically through the curves plotted in Figs. 3, 3, 4, 5, 6, 7, 8, 9, 10, 11 and 12. It is shown from Eq. (12) that there is a direct relation between the function $f'(\xi, \eta)$ and the dimensionless velocity of the Carreau fluid. Hence, these figures allow to analyze the

distributions of the dimensionless velocity, temperature, skin friction coefficient and local Nusselt number.

Figures 3, 4, 5, 6, 7, 8 and 9 exhibit the velocity and temperature distributions (i.e., $f'(\xi, \eta)$ and $\theta(\xi, \eta)$) for various thermo-physical parameters, namely the Carreau fluid parameter (i.e., Weissenberg number) We , the magnetic body force parameter M , the velocity slip parameter S_f , the thermal slip parameter S_T , the Prandtl number Pr , the power law index n and the steam-wise coordinate ξ .

Figures 10, 11 and 12 depict the effects of the parameters M, S_f and S_T on the variation of both the skin friction coefficient and local Nusselt number (i.e., $Gr^{-3/4} C_f$ and $Gr^{-1/4} Nu$) with the steam-wise coordinate ξ for such a Carreau electro-conductive fluid, which is characterized by $n = 0.1, We = 0.3$ and $Pr = 7$

Figure 3 illustrates the influence of the Weissenberg number We on the velocity and temperature distributions. It is shown from Fig. 3a that the dimensionless velocity component is considerably reduced with the increase in the value of the parameter We . This result can be explained by the increase in the relaxation time of the polymer fluid, which creates a resistance to the fluid flow. The Weissenberg number We introduces a kind of nonlinearity to the system. Furthermore, it is noted that the Weissenberg number We is arised in connection with some higher order derivatives in the momentum boundary layer equation, especially in the mixed derivative $We (\partial^2 f / \partial \eta^2)^2 (\partial^3 f / \partial \eta^3)$. From Fig. 3b, it is quite clear that an increase in the Weissenberg number We enhances somewhat the temperature throughout the boundary layer regime.

Figure 4 is plotted to highlight the effect of the magnetic parameter M on the velocity and temperature distributions. From Fig. 4a, it is observed that the velocity profile decreases with the rise in the values of the magnetic parameter M . The presence of a magnetic field in an electrically conducting fluid introduces a drag-like force known as Lorentz force, which acts against the flow, in the case where the magnetic field is applied vertically across the fluid flow. Hence, the magnetic resistive forces allow to slow down the fluid velocity. Moreover, it is found from Fig. 4b that the temperature is increased with the increase in the values of the magnetic parameter M . As a result, the momentum boundary layer thickness is reduced and the temperature throughout the boundary layer increases slightly with the increase in the magnetic parameter M . It is worth mentioning here that the resistance caused by the presence of the external magnetic field will produce the - heat in the system and increase the thermal boundary layer thickness.

Figure 5 exhibits the influence of the effect of the velocity slip parameter S_f on the velocity and temperature distributions. It is seen from Fig. 5a that the flow is

Table 1 Comparison of Nu with the existing works of Molla et al. [32] and Haque et al. [33], in the case where $Pr = 0.7$ and $We = S_f = S_T = M = 0$

ξ (°)	$Pr = 0.7$		
	[32]	[33]	Present solutions
0	0.4576	0.45762	0.45758
10	0.4564	0.45653	0.45690
20	0.4532	0.45336	0.45346
30	0.4479	0.44808	0.44725
40	0.4404	0.44067	0.44309
50	0.4307	0.43107	0.43277
60	0.4188	0.41920	0.41821
70	0.4045	0.40499	0.40318
80	0.3877	0.38828	0.39435
90	0.3683	0.36891	0.37247

Table 2 Impact of S_f , S_T and ξ on $f''(\xi, 0)$, in the case where $Pr = 7$, $We = 0.3$ and $M = 1$

S_f	S_T	$\xi = 0$	$\xi = \pi/6$	$\xi = \pi/4$	$\xi = \pi/3$	$\xi = \pi/2$	$\xi = 2\pi/3$
0	1	0	0.1908	0.2592	0.3473	0.4415	0.4506
0.1		0	0.1858	0.2522	0.3376	0.4280	0.4344
0.2		0	0.1807	0.2453	0.3280	0.4144	0.4182
0.3		0	0.1757	0.2383	0.3183	0.4009	0.4020
0.5		0	0.1657	0.2244	0.2989	0.3738	0.3694
0.8		0	0.1506	0.2036	0.2699	0.3330	0.3204
1		0	0.1406	0.1897	0.2504	0.3058	0.2876
0.5	0	0	0.1871	0.2536	0.3382	0.4241	0.4218
	0.5	0	0.1765	0.2391	0.3187	0.3991	0.3957
	1.5	0	0.1547	0.2096	0.2790	0.3481	0.3427
	2	0	0.1437	0.1945	0.2587	0.3222	0.3157
	2.5	0	0.1324	0.1792	0.2381	0.2958	0.2884
	3	0	0.1210	0.1636	0.2172	0.2690	0.2606

Bold values indicate better results

Table 3 Impact of S_f , S_T and ξ on $-\theta'(\xi, 0)$, in the case where $Pr = 7$, $We = 0.3$ and $M = 1$

S_f	S_T	$\xi = 0$	$\xi = \pi/6$	$\xi = \pi/4$	$\xi = \pi/3$	$\xi = \pi/2$	$\xi = 2\pi/3$
0	1	0.7199	0.7015	0.6857	0.6521	0.5687	0.4466
0.1		0.7326	0.7140	0.6981	0.6641	0.5795	0.4554
0.2		0.7454	0.7266	0.7105	0.6761	0.5904	0.4638
0.3		0.7582	0.7393	0.7229	0.6883	0.6013	0.4727
0.5		0.7839	0.7645	0.7475	0.7125	0.6234	0.4904
0.8		0.8225	0.8026	0.7850	0.7492	0.6563	0.5173
1		0.8483	0.8279	0.8100	0.7726	0.6786	0.5351
0.5	0	0.9259	0.9032	0.8835	0.8421	0.7374	0.5814
	0.5	0.8543	0.8333	0.8151	0.7767	0.6798	0.5355
	1.5	0.7147	0.6979	0.6814	0.6494	0.5678	0.4462
	2	0.6469	0.6308	0.6166	0.5875	0.5134	0.4029
	2.5	0.5804	0.5659	0.5532	0.5272	0.4601	0.3607
	3	0.5154	0.5025	0.4911	0.4680	0.4080	0.3194

Bold values indicate better results

Table 4 Impact of We , M and Pr on $f''(\xi, 0)$, in the case where $S_f = 0.5$, $S_T = 1$ and $\xi = 1$

We	M	$Pr = 7$	$Pr = 10$	$Pr = 20$	$Pr = 25$	$Pr = 50$	$Pr = 75$	$Pr = 100$
0	1	0.2960	0.2730	0.2294	0.2157	0.1749	0.1524	0.1370
0.5		0.3008	0.2769	0.2316	0.2176	0.1762	0.1533	0.1377
1		0.3049	0.2803	0.2341	0.2198	0.1771	0.1541	0.1383
2		0.3122	0.2864	0.2382	0.2234	0.1795	0.1557	0.1393
3		0.3185	0.2916	0.2417	0.2265	0.1815	0.1571	0.1407
4		0.3240	0.2964	0.2449	0.2294	0.1833	0.1584	0.1417
0.3	0	0.3760	0.3444	0.2870	0.2698	0.2194	0.1924	0.1745
	0.5	0.3302	0.3029	0.2529	0.2376	0.1923	0.1677	0.1512
	1	0.2989	0.2753	0.2308	0.2170	0.1757	0.1529	0.1374
	2	0.2538	0.2352	0.1988	0.1872	0.1517	0.1315	0.1175
	3	0.2203	0.2052	0.1745	0.1645	0.1332	0.1149	0.1022
	4	0.1936	0.1809	0.1546	0.1457	0.1177	0.1011	0.0893

Bold values indicate better results

Table 5 Impact of We , M and Pr on $-\theta'(\xi, 0)$, in the case where $S_f = 0.5$, $S_T = 1$ and $\xi = 1$

We	M	$Pr = 7$	$Pr = 10$	$Pr = 20$	$Pr = 25$	$Pr = 50$	$Pr = 75$	$Pr = 100$
0	1	0.7145	0.8098	1.0370	1.1239	1.4513	1.6946	1.8975
	0.5	0.7104	0.8063	1.0322	1.1190	1.4473	1.6911	1.8942
	1	0.7072	0.8028	1.0289	1.1158	1.4430	1.6879	1.8913
	2	0.7012	0.7966	1.0226	1.1095	1.4376	1.6821	1.8846
	3	0.6961	0.7912	1.0168	1.1036	1.4321	1.6769	1.8812
0.3	0	0.8013	0.9019	1.1364	1.2267	1.5630	1.8118	2.0183
	0.5	0.7497	0.8463	1.0747	1.1628	1.4925	1.7373	1.9413
	1	0.7125	0.8089	1.0330	1.1213	1.4489	1.6925	1.8955
	2	0.6568	0.7512	0.9736	1.0593	1.3850	1.6270	1.8289
	3	0.6144	0.7072	0.9277	1.0122	1.3355	1.5762	1.7772
	4	0.5799	0.6710	0.8902	0.9735	1.2928	1.5333	1.7334

Bold values indicate better results

Fig. 3 Effect of the Weissenberg number We on **a** the velocity and **b** temperature profiles, when $n = 0.1$, $Pr = 7$, $M = 1$, $S_f = 0.5$, $S_T = 1$ and $\xi = 1$

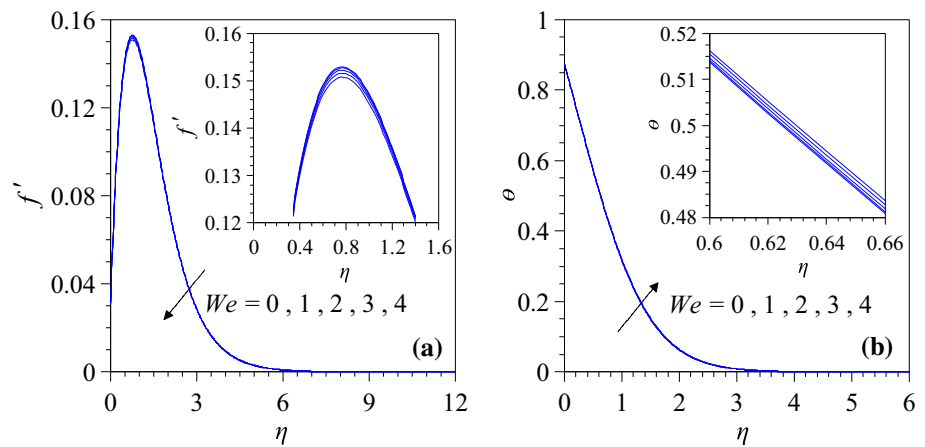
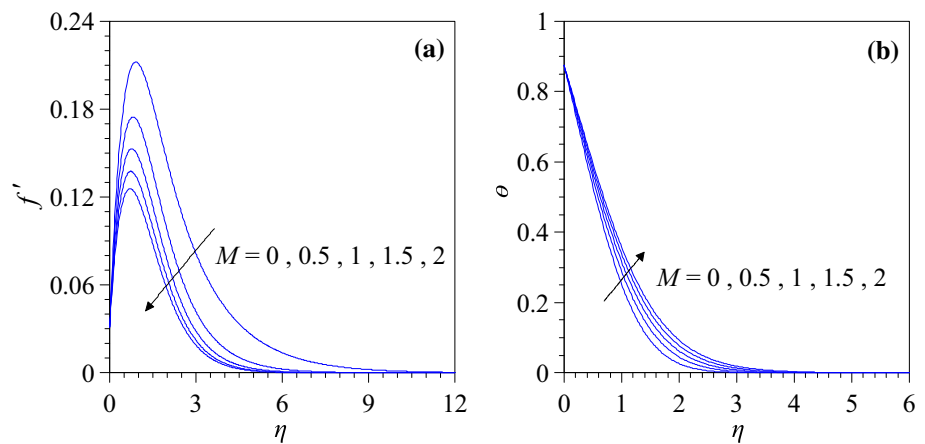


Fig. 4 Effect of the Magnetic parameter M on **a** the velocity and **b** temperature profiles, when $n = 0.1$, $We = 0.3$, $Pr = 7$, $S_f = 0.5$, $S_T = 1$ and $\xi = 1$



markedly accelerated in the vicinity of the sphere surface with the increase in the velocity slip parameter S_f . The velocity profiles plotted in Fig. 5a show the presence of peaks from some distance of the wall. These peaks are taken high values and shifted closer to the sphere wall,

when the value of the velocity slip parameter S_f is increased. Thereafter, the momentum slip induces a notable acceleration in the flow near to the sphere surface and decreases the momentum boundary layer thickness. On the contrary, it is observed that the momentum slip retards

Fig. 5 Effect of the velocity slip parameter S_f on **a** the velocity and **b** temperature profiles, when $n = 0.1$, $We = 0.3$, $Pr = 7$, $M = 1$, $S_T = 1$ and $\zeta = 1$

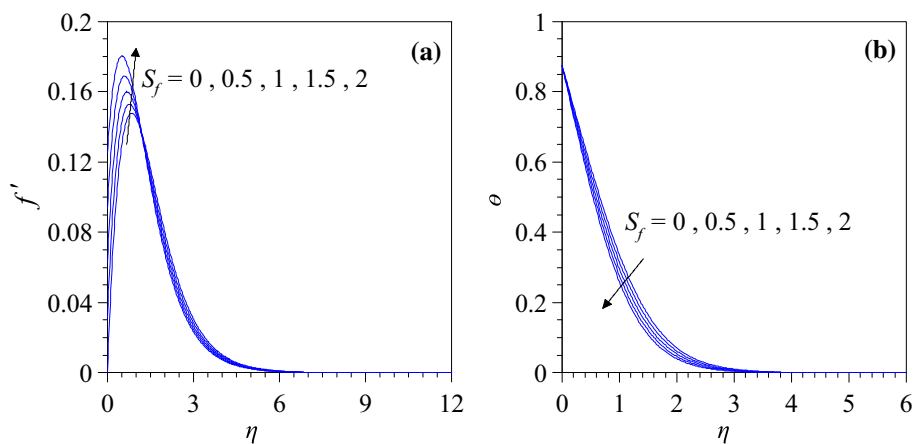


Fig. 6 Effect of the thermal jump parameter S_T on **a** the velocity and **b** temperature profiles, when $n = 0.1$, $We = 0.3$, $Pr = 7$, $M = 1$, $S_f = 0.5$ and $\zeta = 1$

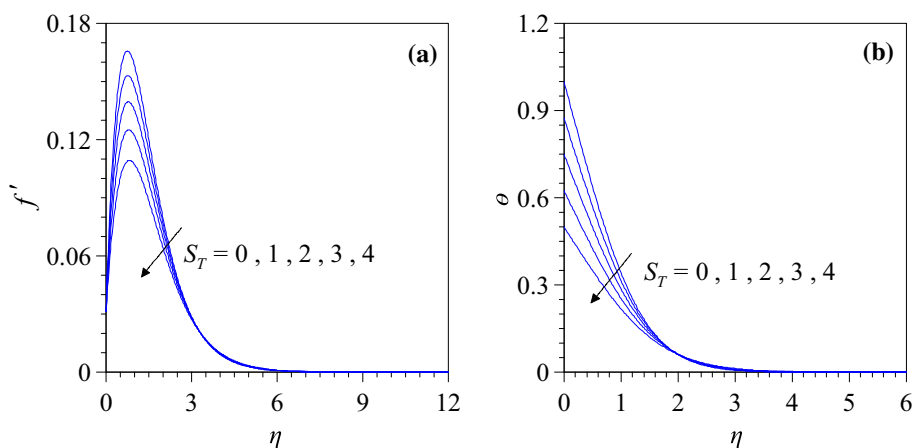
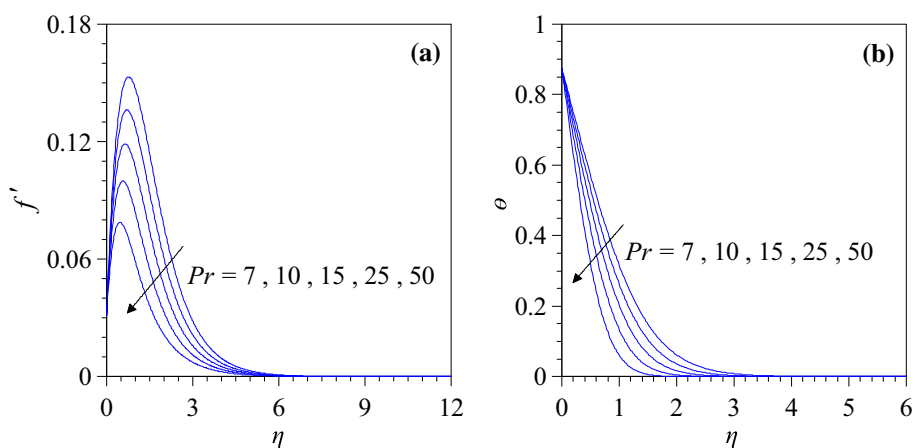


Fig. 7 Effect of the Prandtl number Pr on **a** the velocity and **b** temperature profiles, when $n = 0.1$, $We = 0.3$, $M = 1$, $S_f = 0.5$, $S_T = 1$ and $\zeta = 1$



the fluid motion near and at the infinity boundary condition. Moreover, dragging of the fluid adjacent to the sphere surface is partially transmitted into the fluid, which induces a deceleration near the wall. However, this observation is eliminated and reversed further from the sphere surface. From Fig. 5b, it is found that the temperature profiles decay monotonically from a maximum at the sphere surface to the free stream, so that these profiles is converged at

a large value of transverse coordinate η to the zero value, again showing that a sufficiently large infinity boundary condition has been taken into account during the numerical computations. With greater momentum slip, the temperature in the boundary layer is substantially decreased, and hence the thermal boundary layer thickness is dropped appreciably with the increase in the velocity slip parameter S_f . Therefore, the regime is hottest when the momentum

Fig. 8 Effect of the power law index parameter n on **a** the velocity and **b** temperature profiles, when $We = 0.3$, $Pr = 7$, $S_f = 0.5$, $S_T = 1$ and $\xi = 1$

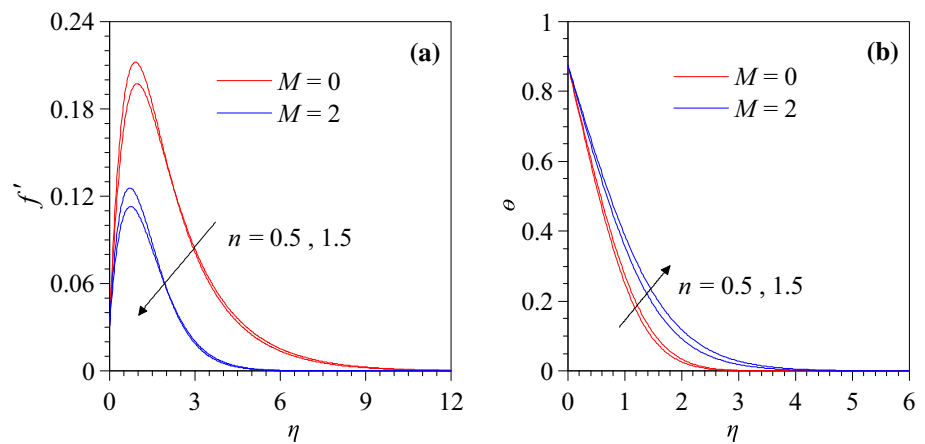


Fig. 9 Effect of steam-wise coordinate ξ on **a** the velocity and **b** temperature profiles, when $n = 0.1$, $We = 0.3$, $Pr = 7$, $M = 1$, $S_f = 0.5$ and $S_T = 1$

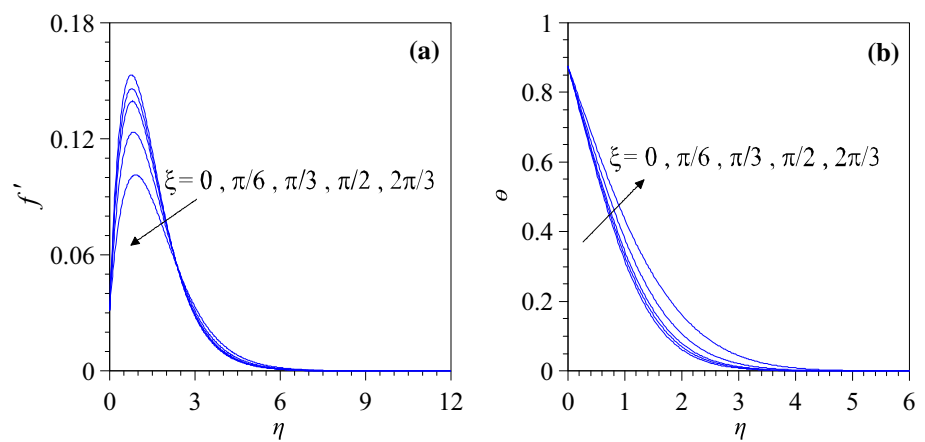
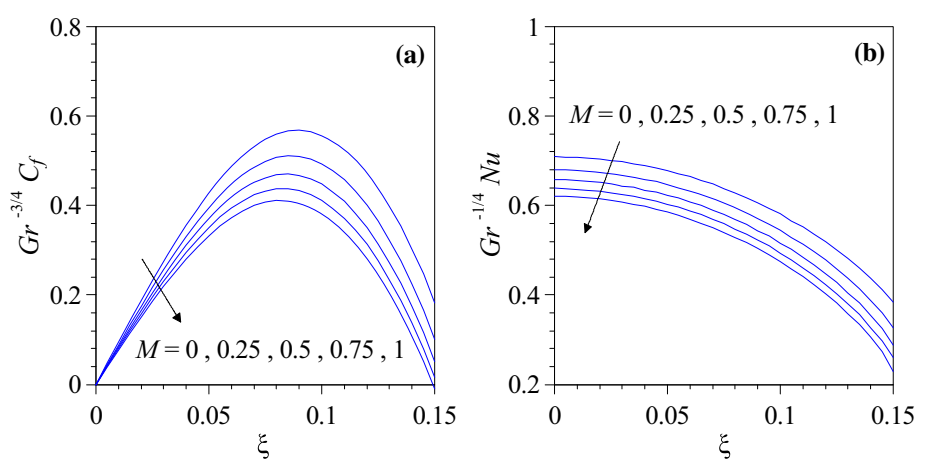


Fig. 10 Effect of the Magnetic parameter M on **a** the skin friction and **b** Nusselt number profiles, when $n = 0.1$, $We = 0.3$, $Pr = 7$, $S_f = 0.5$ and $S_T = 1$



slip is absent (i.e., $S_f = 0$) and coolest with a strong hydrodynamic wall slip.

Figure 6 shows the influence of the thermal slip parameter S_T on the velocity and temperature distributions. From Fig. 6a, b, it is clearly noticed that both the velocity and the temperature are consistently decreased with the increase in the thermal slip parameter S_T in the vicinity of the sphere surface, so that the temperature

becomes strongly depressed at the sphere surface. Hence, an increase in the value of the thermal jump parameter S_T allows to decelerate the flow and cool the boundary layer. It is also found that the momentum and thermal boundary layer thicknesses arise slightly when the thermal slip parameter S_T is increased. Physically, an increase in the thermal slip parameter S_T renders the fluid flow within the boundary layer progressively less sensitive to the heating

Fig. 11 Effect of the velocity slip parameter S_f on **a** the skin friction and **b** Nusselt number profiles, when $n = 0.1$, $We = 0.3$, $Pr = 7$, $M = 1$ and $S_T = 1$

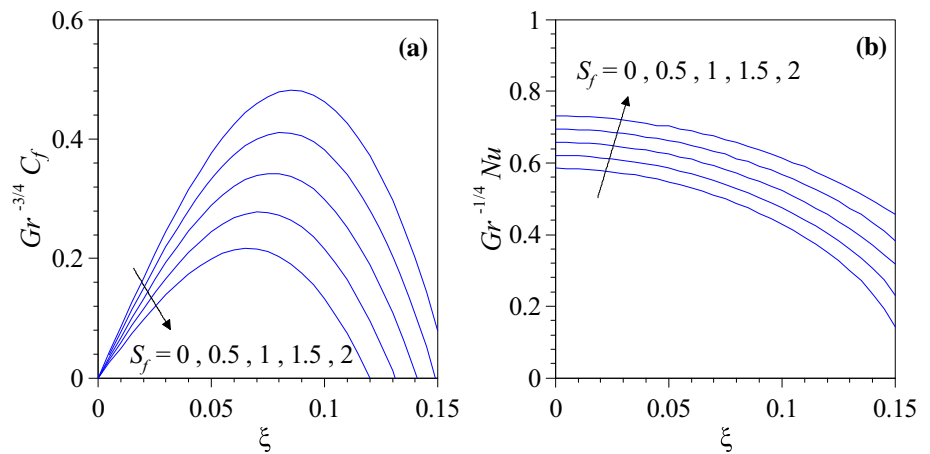
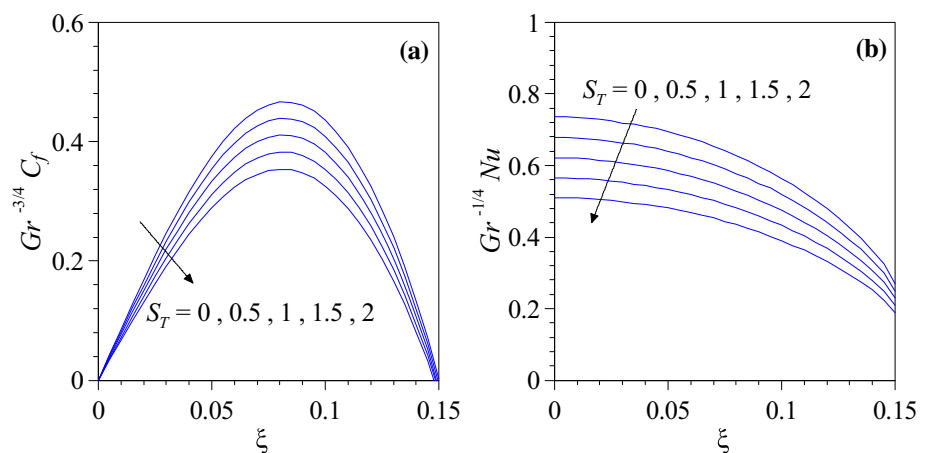


Fig. 12 Effect of the thermal jump parameter S_T on **a** the skin friction and **b** Nusselt number profiles, when $n = 0.1$, $We = 0.3$, $Pr = 7$, $M = 1$ and $S_f = 0.5$



effects at the sphere surface, so that a decreased quantity of thermal energy is transferred from the hot surface to the fluid, producing a fall in the temperature throughout the boundary layer. These results have important implications in the thermal polymer enrobing, since the thermal slip modifies the heat transferred to the polymer material, which in turn alters characteristics of the final product.

Figure 7 represents the velocity and temperature profiles for various values of the Prandtl number Pr . From Fig. 7a, b, it is found that an increase in the Prandtl number Pr decreases both the polymer flow velocity and the temperature throughout the boundary layer. Physically, the Prandtl number Pr represents the ratio of the viscosity to the thermal diffusivity. Hence, the rise in the values of the Prandtl number Pr will cause a large increase in the fluid viscosity, so that the fluid becomes extremely thick, and hence moves so slowly. The most prominent variation in the velocity and temperature distributions arises at intermediate distances from the sphere surface. Furthermore, it is quite clear that the momentum and thermal boundary layers are thinner at large values of the Prandtl number Pr compared with the case where the values of the Prandtl number Pr are taken smaller. This fact is due to the inverse

relation between the Prandtl number Pr and the thermal diffusivity. So, an increase in the Prandtl number Pr prevents spreading a large amount of heat within the boundary layer.

Figure 8 depicts the impact of the power law index parameter n on the velocity and temperature distributions for distinct values of the magnetic parameter M . In the presence or absence of an external magnetic field, it is observed from Fig. 8a that there is an opposite behavior of the power law index parameter n toward the fluid velocity, so that for higher values of the power law index parameter n , the fluid velocity decreases and the thickness of the boundary layer becomes thinner. This result can be explained by the augmentation in the apparent viscosity of the Carreau fluid. Therefore, the fluid flow becomes more resistive, and hence the temperature distribution and the thermal boundary layer thickness are increased as shown in Fig. 8b.

Figure 9 is plotted to examine the impact of the streamwise coordinate ξ on the velocity and temperature distributions. From Fig. 9a, it is quite clear that the velocity of the fluid flow is reduced in the vicinity of the sphere surface, when we move away from the lower stagnation point

Table 6 Numerical values of the quantities $Gr^{-3/4} C_f$ and $Gr^{-1/4} Nu$ for various values of M , S_f and S_T , in the case where $We = 0.3$, $n = 0.1$ and $Pr = 7$

ξ	M	S_f	S_T	$Gr^{-3/4} C_f$	$Gr^{-1/4} Nu$
0.10	0	0.5	1	0.5564	0.5812
	0.25			0.4936	0.5441
	0.5			0.4481	0.5160
	0.75			0.4119	0.4935
0.06	1	0	1	0.4249	0.5301
		0.5		0.3732	0.5697
		1		0.3206	0.6104
		1.5		0.2677	0.6483
0.08	1	0.5	0	0.4664	0.6270
			0.5	0.4387	0.5772
			1	0.4107	0.5290
			1.5	0.3822	0.4822

Bold values indicate better results

$(\xi, \eta) = (0, 0)$. It is also observed that the momentum boundary layer thickness is increased marginally with the stream-wise coordinate ξ . Conversely, it is shown in Fig. 9b that there is an enhancement in both the temperature distribution along the boundary layer and the thermal boundary layer thickness.

The variation of on the engineering quantities $Gr^{-3/4} C_f$ and $Gr^{-1/4} Nu$ of a Carreau fluid versus the stream-wise coordinate ξ for various values of the magnetic parameter M , the velocity slip parameter S_f and the thermal slip parameter S_T are presented graphically in Figs. 10, 11 and 12 and summarized numerically in Table 6, in the case where $n = 0.1$, $We = 0.3$ and $Pr = 7$. From these figures, it is seen that for extensive values of the parameters M , S_f and S_T there is a significant depletion in the local shear stress at the sphere surface. Hence, the presence of an external magnetic source with the momentum and thermal slip conditions allow to minimize the effect of the resulting viscous friction forces at the sphere surface. Furthermore, it is noticed that the local heat transfer rate is reduced when the parameters M and S_T is increased. It is also found that the local heat transfer rate can be enhanced when the parameter S_f is increased.

5 Conclusions

A mathematical model has been developed for the buoyancy driven MHD boundary layer flow of a Carreau fluid over a sphere. The transformed conservation equations have been solved with prescribed boundary conditions using the finite difference implicit Keller-

Box method, which has a second-order accuracy. Excellent convergence and stability characteristics are demonstrated by the Keller-Box scheme, which is capable of solving very strongly nonlinear rheological problems.

The present simulations have shown that:

1. An increase in either the Carreau viscoelastic fluid parameter We , the magnetic parameter M , the thermal slip parameter S_T , the Prandtl number Pr , the power law index n or the stream-wise coordinate ξ allows to decrease the fluid velocity near the sphere surface.
2. The presence of the velocity slip condition S_f allows to increase the fluid velocity near the sphere surface.
3. An increase in either the Carreau viscoelastic fluid parameter We , the magnetic parameter M , the power law index n or the stream-wise coordinate ξ allows to improve the temperature throughout the boundary layer.
4. The temperature distribution throughout the boundary layer can be reduced by the increase in either the velocity slip parameter S_f , the thermal slip parameter S_T or the Prandtl number Pr .
5. The effect of viscous friction at the sphere surface can be minimized by increasing the values of the magnetic parameter M , the velocity slip parameter S_f and the thermal slip parameter S_T .
6. The local heat transfer rate is enhanced with the increase in the velocity slip parameter S_f , while an inverse result is observed when the parameters M and S_T are increased.

Acknowledgements The authors appreciate the constructive comments of the reviewers which led to definite improvement in the paper. The corresponding author Dr. CH. Amanulla is thankful to Mohammed Rafeek Mysore, IT analyst in Tata Consultancy Services (TCS) Miami FL, USA, for his financial support.

References

1. Landau LD, Levich B (1942) Dragging of liquid by a plate. Acta Physicochim USSR 17:42–54
2. Lawrence CJ, Zhou W (1991) Spin coating of non-Newtonian fluids. J Non-Newtonian Fluid Mech 39:137–187
3. Samson Jenekhe A, Schuldt Spencer B (1984) Coating flow of non-Newtonian fluids on a flat rotating disk. Int Eng Chem Fundam 23:432–436
4. Osvaldo Campanella H, Galazzo Jorge L, Cerro Ramón L (1986) Viscous flow on the outside of a horizontal rotating cylinder—II. Dip coating with a non-Newtonian fluid. Chem Eng Sci 41:2707–2713
5. Zevallos GA, Carvalho MS, Pasquali M (2005) Forward roll coating flows of viscoelastic liquids. J Non-Newtonian Fluid Mech 130:96–109
6. Mitsoulis E (1986) Fluid flow and heat transfer in wire coating: a review. Adv Polym Technol 6:467–487

7. Mark JE (1996) Physical properties of polymers handbook. AIP Press Woodbury, New York
8. Hashim Masood K (2017) Critical values in flow patterns of Magneto-Carreau fluid over a circular cylinder with diffusion species: multiple solutions. *J Taiwan Inst Chem Eng* 77:282–292. <https://doi.org/10.1016/j.jtice.2017.04.047>
9. Khan M, Hashim Alshomrani AS (2016) MHD stagnation-point flow of a Carreau fluid and heat transfer in the presence of convective boundary conditions. *PLoS ONE* 11:e0157180
10. Akbar NS, Nadeem S (2014) Carreau fluid model for blood flow through a tapered artery with a stenosis. *Ain Shams Eng J* 5:1307–1316. <https://doi.org/10.1016/j.asej.2014.05.010>
11. Naganthran K, Nazar R (2016) Stability analysis of MHD stagnation-point flow towards a permeable stretching/shrinking surface in a Carreau fluid. *AIP Conf Proc* 1750:030031. <https://doi.org/10.1063/1.4954567>
12. Khan M, Malik MY, Salahuddin T, Khan I (2016) Heat transfer squeezed flow of Carreau fluid over a sensor surface with variable thermal conductivity: a numerical study. *Results Phys* 6:940–945. <https://doi.org/10.1016/j.rinp.2016.10.024>
13. Hayat T, Ullah I, Ahmad B, Alsaedi A (2017) Radiative flow of Carreau liquid in presence of Newtonian heating and chemical reaction. *Results Phys* 7:715–722. <https://doi.org/10.1016/j.rinp.2017.01.019>
14. Krishna PM, Sandeep N, Sharma RP (2017) Computational analysis of plane and parabolic flow of MHD Carreau fluid with buoyancy and exponential heat source effects. *Eur Phys J Plus* 132:202. <https://doi.org/10.1140/epjp/i2017-11469-9>
15. Liu Y, Gehde M (2016) Effects of surface roughness and processing parameters on heat transfer coefficient between polymer and cavity wall during injection molding. *Int J Adv Manuf Technol* 84:1325–1333
16. Hatzikiriakos Savvas G, Mitsoulis Evan (2009) Slip effects in tapered dies. *Polym Eng Sci* 49:1960–1969
17. Amanulla CH, Nagendra N, Surya Narayana Reddy M (2017) Numerical study of thermal and momentum slip effects on MHD williamson nanofluid from an isothermal sphere. *J Nanofluids* 6:1111–1126. <https://doi.org/10.1166/jon.2017.1405>
18. Amanulla CH, Nagendra N, Surya Narayana Reddy M, Subba Rao A, Bég OA (2017) Mathematical study of non-Newtonian nanofluid transport phenomena from an isothermal sphere. *Front Heat Mass Transf* 8:29. <https://doi.org/10.5098/hmt.8.29>
19. Sparrow EM, Lin SH (1962) Laminar heat transfer in tubes under slip-flow conditions. *ASME J Heat Transf* 84:363–639
20. Khellaf K, Lauriat G (2000) Numerical study of heat transfer in a non-Newtonian Carreau-fluid between rotating concentric vertical cylinders. *J Non-Newtonian Fluid Mech* 89:45–61
21. Khan, Hashim M, Hussain M, Azam M (2016) Magnetohydrodynamic flow of Carreau fluid over a convectively heated surface in the presence of non-linear radiation. *J Magn Magn Mater* 412:63–68. <https://doi.org/10.1016/j.jmmm.2016.03.077>
22. Raju CSK, Sandeep N (2016) Falkner–Skan flow of a magnetic-Carreau fluid past a wedge in the presence of cross diffusion effects. *Eur Phys J Plus* 131:267. <https://doi.org/10.1140/epjp/i2016-16267-3>
23. Akbar NS, Nadeem S, UI Haq. R, Ye S (2014) MHD stagnation point flow of Carreau fluid toward a permeable shrinking sheet: dual solutions. *Ain Shams Eng J* 5:1233–1239. <https://doi.org/10.1016/j.asej.2014.05.006>
24. Reddy MG, Sandeep N (2016) Heat and mass transfer in radiative MHD Carreau fluid with cross diffusion. *Ain Shams Eng J*. <https://doi.org/10.1016/j.asej.2016.06.012>
25. Black WB (2000) Wall slip and boundary effects in polymer shear flows, Ph.D. Thesis, Chemical Engineering, University of Wisconsin, Madison
26. Wang SQ, Drda PA, Inn YW (1996) Exploring molecular origins of sharkskin, partial slip, and slope change in flow curves of linear low density polyethylene. *J Rheol* 40:875–898
27. Piau JM, Kissi NE, Toussaint F, Mezghani A (1995) Distortions of polymer extrudates and their elimination using slippery surfaces. *Rheol Acta* 34:40–57
28. Piau JM, Kissi NE (1994) Measurement and modelling of friction in polymer melts during macroscopic slip at the wall. *J Non-Newtonian Fluid Mech* 54:121–142
29. Lim FJ, Schowalter WR (1989) Wall slip of narrow molecular weight distribution polybutadienes. *J Rheol* 33:1359–1382
30. Hatzikiriakos SG, Kalogerakis N (1994) A dynamic slip velocity model for molten polymers based on a network kinetic theory. *Rheol Acta* 33:38–47
31. Sparrow EM, Lin SH (1962) Laminar heat transfer in tubes under slip-flow conditions. *ASME J Heat Transf* 84:363–639
32. Ali Y, Khan AA (2018) Exact solution of magnetohydrodynamic slip flow a heat transfer over an oscillating and translating porous plate. *Discrete Contin Dyn Syst Ser S* 11:595–606
33. Aziz A, Ali Y, Aziz T, Siddique JI (2015) Heat transfer analysis for stationary boundary layer slip flow of a power-law fluid in a darcy porous medium with plate suction/injection. *PLoS ONE* 10(9):e0138855. <https://doi.org/10.1371/journal.pone.0138855>
34. Ellahi R, Bhatti MM, Pop I (2016) Effects of hall and ion slip on MHD peristaltic flow of Jeffrey fluid in a non-uniform rectangular duct. *Int J Numer Meth Heat Fluid Flow* 26:1802–1820. <https://doi.org/10.1108/HFF-02-2015-0045>
35. Amanulla CH, Nagendra N, Suryanarayana Reddy M (2018) Numerical simulations on magnetohydrodynamic non-newtonian nanofluid flow over a semi-infinite vertical surface with slip effect. *J Nanofluids* 7:718–730. <https://doi.org/10.1166/jon.2018.1499>
36. Amanulla CH, Nagendra N, Suryanarayana Reddy M (2018) Numerical simulation of slip influence on the flow of a MHD williamson fluid over a vertical convective surface. *Nonlinear Eng*. <https://doi.org/10.1515/nleng-2017-0079>
37. Amanulla CH, Nagendra N, Suryanarayana Reddy M (2017) MHD flow and heat transfer in a williamson fluid from a vertical permeable cone with thermal and momentum slip effects: a mathematical study. *Front Heat Mass Transf* 8:40. <https://doi.org/10.5098/hmt.8.40>
38. Amanulla CH, Nagendra N, Suryanarayana Reddy M (2017) Thermal and momentum slip effects on hydromagnetic convection flow of a williamson fluid past a vertical truncated cone. *Front Heat Mass Transf* 9:22. <https://doi.org/10.5809/hmt.9.22>
39. Amanulla CH, Nagendra N, Suryanarayana Reddy M (2018) Computational analysis of non-newtonian boundary layer flow of nanofluid past a semi-infinite vertical plate with partial slip. *Nonlinear Eng* 7:29–43. <https://doi.org/10.1515/nleng-2017-0055>
40. Amanulla CH, Nagendra N, Suryanarayana Reddy M (2017) Multiple slip effects on MHD and heat transfer in a jeffery fluid over an inclined vertical plate. *Int J Pure Appl Math* 113:137–145
41. Molla MM, Taher MA, Chowdhury MMK, Hossain MA (2005) Magnetohydrodynamic natural convection flow on a sphere in presence of heat generation. *Nonlinear Anal Model Control* 10:349
42. Haque MR, Alam MM, Ali MM, Karim R (2015) Effects of viscous dissipation on natural convection flow over a sphere with temperature dependent thermal conductivity in presence of heat generation. *Procedia Eng* 105:215
43. Cebeci T, Bradshaw P (1984) Physical and computational aspects of convective heat transfer. Springer, New York
44. Keller HB (1970) A new difference method for parabolic problems. In: Bramble J (ed) Numerical methods for partial differential equations. Academic Press, New York

45. Rao SA, Amanulla CH, Nagendra N, Surya Narayana Reddy M, Bég OA (2017) Computational analysis of non-newtonian boundary layer flow of nanofluid past a vertical plate with partial slip. *Model Meas Control B* 86:271–295
46. Rao SA, Amanulla CH, Nagendra N, Bég OA, Kadir A (2017) Hydromagnetic flow and heat transfer in a williamson non-Newtonian fluid from a horizontal circular cylinder with Newtonian heating. *Int J Appl Comput Math* 3:3389–3409. <https://doi.org/10.1007/s40819-017-0304-x>
47. Rao SA, Amanulla CH, Nagendra N, Surya Narayana Reddy M, Bég OA (2018) Hydromagnetic non-Newtonian nanofluid transport phenomena past an isothermal vertical cone with partial slip: aerospace nanomaterial enrobing simulation. *Heat Trans Asian Res* 47:203–230. <https://doi.org/10.1002/htj.21299>
48. Amanulla CH, Nagendra N, Rao AS, Bég OA, Kadir A (2018) Numerical exploration of thermal radiation and biot number effects on the flow of a non-Newtonian MHD Williamson fluid over a vertical convective surface. *Heat Trans Asian Res* 47:286–304. <https://doi.org/10.1002/htj.21303>